Theoretical evidence of spin-orbital-entangled J eff = 1 2 state in the 3d transition metal oxide CuAl 2 O 4

Article · October 2019

DOI: 10.1103/PhysRevB.100.161104

9 authors, including:

Santu Baidya
Rutgers, The State University of New Jersey

Hwanbeom Cho
University of Oxford

S. V. Streltsov
Institute of Metal Physics

Je-Geun Park
Seoul National University

Rapid Communications

Theoretical evidence of spin-orbital-entangled $J_{\mathrm{eff}} = \frac{1}{2}$ state in the 3*d* transition metal oxide $CuAl_2O_4$

Choong H. Kim,[1,2,*] Santu Baidya,[1,2] Hwanbeom Cho,[1,2] Vladimir V. Gapontsev,[3] Sergey V. Streltsov,[3,4] Daniel I. Khomskii,[5] Je-Geun Park,[1,2] Ara Go,[6,†] and Hosub Jin[7,‡]

[1]*Center for Correlated Electron Systems, Institute for Basic Science (IBS), Seoul 08826, Republic of Korea*
[2]*Department of Physics and Astronomy, Seoul National University, Seoul 08826, Republic of Korea*
[3]*M. N. Miheev Institute of Metal Physics of Ural Branch of Russian Academy of Sciences, 620137 Ekaterinburg, Russia*
[4]*Ural Federal University, 620002 Ekaterinburg, Russia*
[5]*II. Physikalisches Institut, Universität zu Köln, D-50937 Köln, Germany*
[6]*Center for Theoretical Physics of Complex Systems, Institute for Basic Science (IBS), Daejeon 34126, Republic of Korea*
[7]*Department of Physics, Ulsan National Institute of Science and Technology (UNIST), Ulsan 44919, Republic of Korea*

(Received 7 May 2019; revised manuscript received 18 August 2019; published 4 October 2019)

The spin-orbital-entangled Kramers doublet, known as the $J_{\mathrm{eff}} = 1/2$ pseudospin driven by large spin-orbit coupling (SOC), appears in layered iridates and α-$RuCl_3$, manifesting a relativistic Mott insulating phase. Such entanglement, however, seems barely attainable in 3*d* transition metal oxides, where the SOC is small and the orbital angular momentum is easily quenched. Based on the density-functional-theory calculations, we report the $CuAl_2O_4$ spinel as the possible example of a $J_{\mathrm{eff}} = 1/2$ Mott insulator in 3*d* transition metal compounds. With the help of strong electron correlations, the $J_{\mathrm{eff}} = 1/2$ state can survive the competition with an orbital-momentum-quenched $S = 1/2$ state in the d^9 configuration of CuO_4 tetrahedron. From the dynamical mean-field theory calculations, the electron-addition spectra probing unoccupied states are well described by the $j_{\mathrm{eff}} = 1/2$ hole state, whereas electron-removal spectra have a rich multiplet structure. The fully relativistic entity found in $CuAl_2O_4$ provides insight into the untapped regime where the spin-orbital-entangled Kramers pair coexists with strong electron correlation.

DOI: 10.1103/PhysRevB.100.161104

Transition metal oxides exhibit various competing phases and exotic phenomena depending on how they react to the rich degeneracy of the *d* orbital [1–3]. Spin-orbit coupling (SOC) reduces this degeneracy in a different way by providing a spin-orbital-entangled ground state. In particular, the spin-orbital-entangled $J_{\mathrm{eff}} = 1/2$ Kramers doublet has emerged in the 4*d* and 5*d* transition metal compounds with the t_{2g}^5 configuration due to a large atomic spin-orbit coupling (SOC) assisted by moderate electron correlation [4–8]. A variety of novel phenomena has also risen from the $J_{\mathrm{eff}} = 1/2$ state, including a 5*d* analog to a high-T_c cuprate in a square lattice [9,10], topological insulators [11,12], the Kitaev model [6,8,13–15], Weyl semimetals [16], axion insulators [17], and so on [18]. It is interesting to ask how the spin-orbital-entangled state behaves under strong electron correlation [19]. However, this question remains hypothetical, simply because no transition metals can possibly possess both large SOC and strong electron correlation simultaneously. If we take large SOC strength as a prerequisite for the spin-orbital entanglement in the t_{2g}^5 configuration [20], the intriguing strongly correlated $J_{\mathrm{eff}} = 1/2$ state in real materials seems impractical. The Co^{2+} environment has been suggested as a promising candidate for the strongly correlated spin-orbital-entangled state [21,22], but it is yet to be confirmed.

A simple atomic t_{2g}^5 model, in which five electrons occupying the triply degenerate t_{2g} orbital are under strong Coulomb interactions, can give a hint of how to realize the strongly correlated $J_{\mathrm{eff}} = 1/2$ state, even with small SOC. A nonzero SOC within the atomic t_{2g}^5 model favors the $J_{\mathrm{eff}} = 1/2$ doublet as its ground state [23]. Instead of considering the complicated multiplet structure composed of five electrons, the single hole in the atomic t_{2g}^5 model is represented by a simple noninteracting Hamiltonian that reads $\mathcal{H} = \lambda \mathbf{l}_{\mathrm{eff}} \cdot \mathbf{s} + \Delta (l_{\mathrm{eff}}^z)^2$, where λ is the atomic SOC and Δ is the tetragonal crystal field induced by Jahn-Teller distortion. Note that hereafter j_{eff}, l_{eff}, and s (J_{eff}, L_{eff}, and S) stand for single-particle (multiparticle) total, orbital, and spin angular momenta, respectively. The lowest eigenstate of the single hole is Kramers doublet, written as

$$|\psi_\pm\rangle = \sqrt{\alpha}\,|l_{\mathrm{eff}}^z = 0\rangle|\pm\rangle + \sqrt{1-\alpha}\,|l_{\mathrm{eff}}^z = \pm 1\rangle|\mp\rangle, \qquad (1)$$

where $|l_{\mathrm{eff}}^z = 0\rangle = |d_{xy}\rangle$, $|l_{\mathrm{eff}}^z = \pm 1\rangle = -\frac{1}{\sqrt{2}}(i|d_{zx}\rangle \pm |d_{yz}\rangle)$, and $|\pm\rangle$ denotes the spin-1/2 spinor [8]. Once Jahn-Teller distortion is dominant ($\Delta \gg \lambda$), the orbital degeneracy is lifted and the orbital angular momentum is quenched; thus, we end up with the spin-only $S = 1/2$ state ($\alpha = 1$) accompanied by the symmetry-lowering tetragonal distortion, which frequently occurs among 3*d* transition metal oxides. In the strong SOC limit or small Jahn-Teller limit, the spin-orbital-entangled $J_{\mathrm{eff}} = 1/2$ state ($\alpha = 1/3$) arises while preserving

*chkim82@snu.ac.kr
†arago@ibs.re.kr
‡hsjin@unist.ac.kr

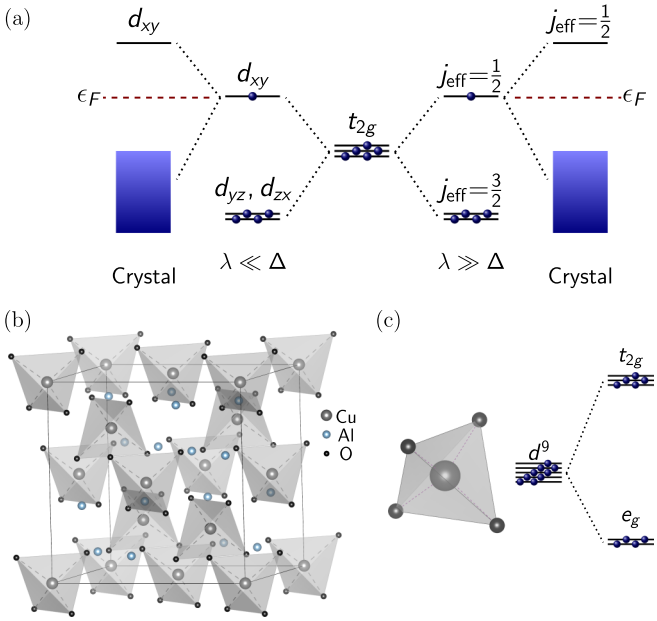

FIG. 1. (a) Two possible ground states from the competition between Jahn-Teller distortion (Δ) and spin-orbit coupling (λ), resulting in $J_{\rm eff} = 1/2$ and $S = 1/2$ states, respectively. (b) The crystal structure of $CuAl_2O_4$. The gray, light blue, and black spheres represent Cu, Al, and O atoms, respectively. The Cu atoms surrounded by the O tetrahedron form a diamond lattice. (c) The atomic energy level diagram of the Cu^{2+} ion in the tetrahedral crystal field.

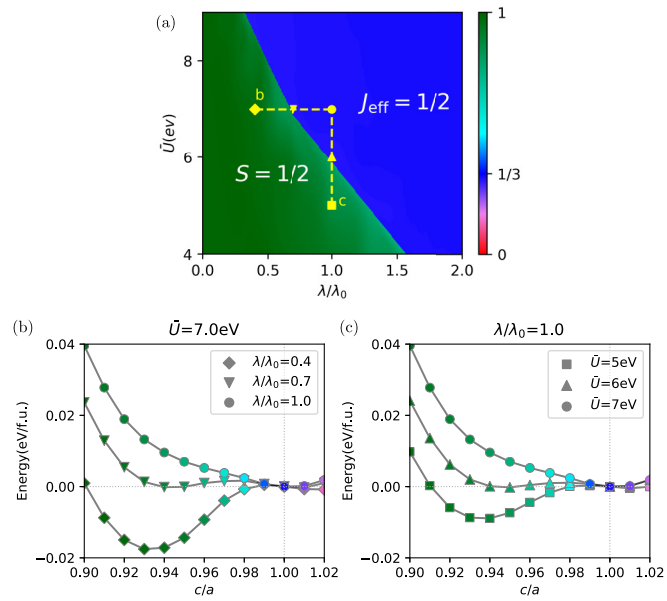

FIG. 2. Phase diagram of $CuAl_2O_4$ from density-functional-theory calculations. (a) The phase diagram as a function of Coulomb interaction ($\bar{U}$) and spin-orbit coupling (λ). (b), (c) Total-energy curve vs c/a with (b) varying $\bar{U}$, fixed λ and (c) varying λ, fixed $\bar{U}$. Different symbols of each energy curve indicate the corresponding parameters set in the phase diagram (a). Color schemes denote α values for given solutions.

the cubic symmetry. When the atomic t_{2g}^5 is embedded in a crystal, two limiting solutions are possible due to the competition between the Jahn-Teller distortions and SOC [Fig. 1(a)]. Therefore, strong electron correlation and the narrow bandwidth of d orbitals in a cubic environment are a simple recipe for the crystalline realization of the atomic t_{2g}^5 model and, thus, for the strongly correlated $J_{\rm eff} = 1/2$ state.

In this Rapid Communication, we report the density-functional-theory (DFT) and dynamical mean-field theory (DMFT) calculation results to demonstrate that the $CuAl_2O_4$ spinel represents the strongly correlated $J_{\rm eff} = 1/2$ Mott phase by hosting the crystalline version of the atomic t_{2g}^5 model. Spin-orbital entanglement in this weak SOC limit is ascribed to the tetrahedrally coordinated t_{2g}^5 in the isolated CuO_4. Because t_{2g} orbitals are not directed to the ligands in tetrahedra, the weak d-p hybridization in CuO_4 reduces the energy gain from the Jahn-Teller distortions and makes the quenching of the orbital angular momentum unlikely. And disconnected tetrahedra reduce the bandwidth of $3d$ orbitals, approaching the atomic t_{2g}^5 limit. Cooperating with large electron correlation, the $J_{\rm eff} = 1/2$ ground state from the $L_{\rm eff} = 1$ orbital and $S = 1/2$ spin angular momenta are stabilized even with the small strength of the bare SOC λ_0 ($\sim$50 meV) of Cu d orbitals. In the strongly correlated $J_{\rm eff} = 1/2$ state, many-body multiplets and a one-particle state appear concurrently in the hole and electron excitation spectra of $CuAl_2O_4$, respectively.

Our total-energy and electronic structure calculations were based on DFT within the Perdew-Burke-Ernzerhof revised for solids (PBEsol) functionals [24], as implemented in ELK code [25]. Brillouin zone integrations were performed using 6×6×6 grid sampling; the basis size was determined by $RK_{\rm max} = 9.0$. We fully optimized the structure with the force criterion of 5×10^{-4} eV/Å. The simplified rotationally invariant DFT+U formalism by Dudarev *et al.* [26] was adopted in the DFT+U+SOC calculations. For the magnetic structure, we employed a collinear Néel antiferromagnetic order in which the moments were aligned along the c axis.

U-λ phase diagram. $CuAl_2O_4$ is one of the rare normal spinel cuprates with Cu^{2+} at the tetrahedral site [Fig. 1(b)]. Recent structure analysis from x-ray and neutron powder diffraction data confirmed that it shows the cubic symmetry with $c/a = 1$ (space group Fd-$3m$, no. 227) [27]. In these spinel cuprates, the well-isolated CuO_4 tetrahedra form a diamond lattice. In the cubic crystal field of ligand tetrahedra, the d^9 electrons in the Cu^{2+} ion fully occupy the e_g orbitals, leaving a single hole in the t_{2g} subshell [Fig. 1(c)]. There is no common oxygen shared by the neighboring CuO_4 tetrahedra. This drives the system closer to the atomic t_{2g}^5 limit, with a small d-orbital bandwidth and strong electron correlations. The small energy gain from the Jahn-Teller distortion of the tetrahedron cage makes $CuAl_2O_4$ a promising candidate to host the $J_{\rm eff} = 1/2$ state in $3d$ transition metal oxides.

We explored the DFT phase diagram of $CuAl_2O_4$ by plotting α defined in Eq. (1) as a function of $\bar{U}$ and λ [Fig. 2(a)]. For the given value of $\bar{U}$ and λ, we investigated the global minimum solution by varying volume V and tetragonal distortion c/a. α has been extracted from the muffin tin orbital basis of a single-hole wave function. The phase diagram is divided into blue and green regions that correspond to the spin-orbital-entangled $J_{\rm eff} = 1/2$ ($\alpha \sim 1/3$, $c/a \sim 1$) and the Jahn-Teller distorted $S = 1/2$ ($\alpha \sim 1$, $c/a < 1$) states,

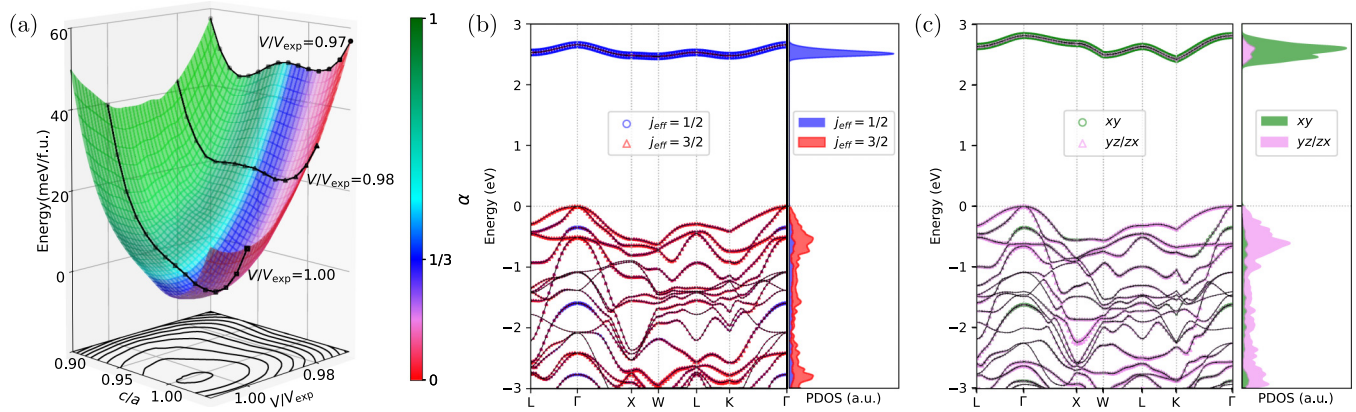

FIG. 3. DFT total-energy landscape and two competing phases. (a) Total-energy landscape as a function of $V/V_{\rm exp}$ and c/a with $U = 7$ eV and $\lambda/\lambda_0 = 1$. (b), (c) Band structure and projected density of states (PDOS) for (b) $V/V_{\rm exp} = 1.0025$ and $c/a = 1.00$ and (c) $V/V_{\rm exp} = 0.970$ and $c/a = 0.93$, corresponding to $J_{\rm eff} = 1/2$ and $S = 1/2$ states, respectively.

respectively. The competition between SOC and Jahn-Teller distortion results in the separation of two distinct solutions. As correlation strength increases, the phase boundary shifts toward the smaller λ, demonstrating that the SOC is enhanced effectively by electron correlation [28,29] and the cubic $J_{\rm eff} = 1/2$ state is stabilized. In Fig. 2(b), the total-energy curves are depicted with a fixed value of $\bar{U}$ (=7 eV) and varying λ. For small SOC, two local minima appear in the total-energy curves at $c/a \sim 0.93$ and $c/a \sim 1$, corresponding to the $S = 1/2$ and $J_{\rm eff} = 1/2$ states, respectively. For nominal SOC strength ($\lambda/\lambda_0 = 0.4$), the $S = 1/2$ state at $c/a = 0.93$ has the lowest energy. Increasing λ stabilizes the local minimum at $c/a \sim 1$ and simultaneously destabilizes the one at $c/a < 1$, leading to a discontinuous transition of the energy minimum from tetragonal $S = 1/2$ to cubic $J_{\rm eff} = 1/2$ states. Similar behavior occurs in the total-energy curves with a fixed λ ($=\lambda_0$) and varying $\bar{U}$; increasing $\bar{U}$ also tends to make the $J_{\rm eff} = 1/2$ state more stable than the $S = 1/2$ state [Fig. 2(c)]. The strong electron correlation helps the small SOC of the Cu d orbital to overcome the Jahn-Teller distortion, enabling the spin-orbital-entangled ground state.

A reasonable value of the correlation strength could be estimated by Cococcioni's linear response approach [30]. In this approach, the response function is $\chi = \frac{\partial n}{\partial \mu}$, where μ is the potential shift and n is the number of electrons on the Hubbard atom. The effective interaction parameter $\bar{U}$ can be obtained by inverting the self-consistent response function and subtracting out the bare (noninteracting) response:

$$\bar{U} = \left(\chi_0^{-1} - \chi^{-1}\right). \tag{2}$$

We obtained $\bar{U} \sim 9$ eV for Cu $3d$ orbitals within this formalism. From the phase diagram, the critical value of $\bar{U}$ for the $J_{\rm eff} = 1/2$ state is about 6 eV, thereby, the $J_{\rm eff} = 1/2$ state could be a plausible ground state of $CuAl_2O_4$.

Total-energy landscape. For $\bar{U} = 7$ eV and $\lambda/\lambda_0 = 1$, we have investigated the total-energy landscape as a function of $V/V_{\rm exp}$ and c/a. As shown in Fig. 3(a), the only stable (and thus global) minimum solution occurs at $V/V_{\rm exp} = 1.0025$ and $c/a = 1$, whose structural properties are consistent with the previous experimental results [27]. The electronic structure and projected density of state (PDOS) at $V/V_{\rm exp} = 1$, $c/a = 1$ is shown in Fig. 3(b). In the band structure, the unoccupied band above the Fermi level can be perfectly projected onto the $j_{\rm eff} = 1/2$ doublet with $\alpha = 0.32$. Since the unoccupied state in the t_{2g}^5 configuration basically represents a single hole, the electron-addition spectra are well described by the spin-orbital-entangled doublet. On the other hand, the electron-removal spectra form a many-body multiplet structure, resulting in the mixture of $j_{\rm eff} = 1/2$ and $3/2$ components in the PDOS plot. This differs from the common expectation for the weakly correlated $J_{\rm eff} = 1/2$ state, for example, realized in Sr_2IrO_4. The multiplet effects appearing in the electron spectrum of $CuAl_2O_4$ become clear in the DMFT calculations shown later.

Even though there is no other stable solution, the total-energy landscape interestingly suggests that a possible Jahn-Teller distorted $S = 1/2$ state might be stabilized under high pressure. At higher pressure, the Cu-O bond length gets shorter, giving rise to larger crystal-field splittings induced by Jahn-Teller distortions. By constraining the volume decreased by 3%, the $S = 1/2$ state at $c/a = 0.93$ has a lower energy than the $J_{\rm eff} = 1/2$ state at $c/a = 1$. Therefore, the two distinct $J_{\rm eff} = 1/2$ and $S = 1/2$ phases can be realized with the same sample by applying pressure values of the experimentally accessible range. The electronic structure of the Jahn-Teller distorted $S = 1/2$ state at $V/V_{\rm exp} = 0.97$, $c/a = 0.93$ is shown in Fig. 3(c). Due to the large tetragonal distortion, the single hole spectrum of the unoccupied t_{2g} bands is mostly composed of the d_{xy} orbital with $\alpha = 0.89$.

DMFT calculations. We also conducted DMFT calculations on top of the DFT-based Wannier Hamiltonian to clarify how robust the $J_{\rm eff}$-ness is under quantum fluctuations. Maximally localized Wannier functions [31] were obtained from the DFT full Cu $3d$+oxygen $2p$ bands in the absence of U and SOC. As such, SOC and the rotationally invariant local Coulomb interaction at each Cu ion were treated by DMFT, where the double-counting correction was applied using the fully localized limit scheme [32]. The correlations involving e_g orbitals were calculated by the Hartree-Fock approximation and the oxygen orbitals were assumed to be noninteracting [33,34]. We employed the exact diagonalization

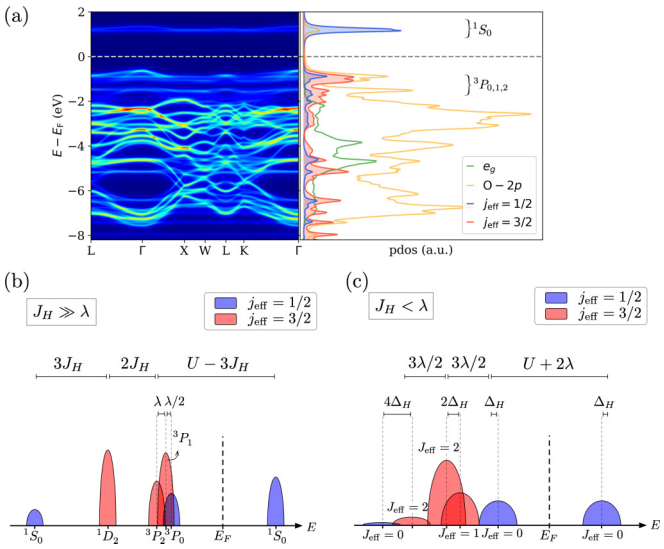

FIG. 4. Multiplets in dynamical mean-field theory (DMFT) calculations. (a) Spectral weights and PDOS from DMFT calculations for $U = 8$ eV, $J_H = 1$ eV, $\lambda = 0.05$ eV. While the spectral gap is roughly proportional to U, the splitting of the hole spectra below the Fermi level depends on λ and $J_{\rm H}$. Schematic illustration of the single-electron/hole excitation spectra from (b) the strongly correlated ($J_{\rm H} \gg \lambda$) and (c) the weakly correlated ($J_{\rm H} < \lambda$) $J_{\rm eff} = 1/2$ ground state. In (c), $\Delta_{\rm H} = 3J_{\rm H}/2$ is used for simplicity.

(ED) [35] as an impurity solver for the zero-temperature DMFT calculations.

We present the DMFT spectral function and PDOS in Fig. 4(a) for a realistic parameter set ($U = 8$ eV, $J_{\rm H} = 1$ eV, and $\lambda = 50$ meV). First of all, we note that the strong $j_{\rm eff} = 1/2$ hole character is also manifested in the DMFT calculation, indicating that the $J_{\rm eff} = 1/2$ state is stable with respect to local quantum fluctuations. The states below the Fermi level exhibit an additional dynamic weight transfer originating from multiplets focusing on the t_{2g} manifold just below the Fermi level; the lowest $t_{2g}^5 \rightarrow t_{2g}^4$ excitation spectra show a mixture of $j_{\rm eff} = 1/2$ and 3/2 characters. This reveals a signature of the strongly correlated $J_{\rm eff} = 1/2$ state obeying the *LS*-coupling scheme, which is distinct from the weakly correlated counterpart such as Sr_2IrO_4 close to the jj-coupling regime.

The weight distribution can be understood by the atomic t_{2g}^5 model with dominating Hund's coupling $J_{\rm H} \gg \lambda$ in Fig. 4(b). In the atomic model, the lowest peak below the Fermi level is composed of three overlapping subpeak structures, denoted by $^3P_0$, $^3P_1$, and $^3P_2$. Each subpeak is categorized by either $j_{\rm eff} = 1/2$ ($^3P_0$) or $j_{\rm eff} = 3/2$ ($^3P_1$, $^3P_2$); the mixture of the $j_{\rm eff} = 1/2$ and 3/2 components in the lowest hole excitation shows the close correspondence between the DMFT spectral function and the atomic multiplet description. (This behavior becomes even clearer in an independent t_{2g}-only DMFT calculation, excluding the e_g and oxygen contribution, as shown in the Supplemental Material [36].) This excitation spectra is further highlighted by comparison with the case of iridates. We investigated the t_{2g}^5 atomic model with a strong SOC regime ($\lambda > J_{\rm H}$) in Fig. 4(c) that can be compared to the $J_{\rm eff} = 1/2$ state in 5*d* iridates [4]. In this strong SOC regime closer to the jj-coupling scheme, electron-removal spectra exhibit two prominent peaks, clearly separated by the large SOC and categorized by $j_{\rm eff} = 1/2$ and $j_{\rm eff} = 3/2$ character, respectively. This feature is reflected in the previous experimental and theoretical reports in Sr_2IrO_4 [4,20,37–39], where the DFT single-particle band structure provides a reasonable description given that multiplet effects are less important in this parameter range. (See the Supplemental Material [36] for the hole excitation spectrum of the atomic t_{2g}^5 model over the whole parameter range.)

Under the cubic symmetry, the SOC puts a single hole in the t_{2g}^5 configuration into the $j_{\rm eff} = 1/2$ state to lower the energy and, therefore, the ground state becomes $J_{\rm eff} = 1/2$. As a result, the $J_{\rm eff} = 1/2$ ground state is represented by the unoccupied $j_{\rm eff} = 1/2$ state in the band structure. But the occupied spectrum of the $J_{\rm eff} = 1/2$ states in the jj- and *LS*-coupling regimes behave very differently from each other. In the jj-coupling scheme ($\lambda > J_{\rm H}$), the occupied states are well described by the single-particle picture. Then we can see the clear separation between the $j_{\rm eff} = 1/2$ and $j_{\rm eff} = 3/2$ states of the occupied bands, as previously shown in iridates. On the other hand, however, the single-particle description is no longer valid in the *LS*-coupling scheme ($\lambda \ll J_{\rm H}$) to explain the occupied spectrum, and thus t_{2g}^4 multiplet structures are inevitable. This is an example of the emerging "strongly correlated" $J_{\rm eff} = 1/2$ state of $CuAl_2O_4$ in which the occupied spectrum is governed by the *LS*-coupling scheme.

Recently, Nirmala and co-workers reported the magnetic susceptibility as well as heat-capacity data and found no signature of long-range magnetic order down to 0.4 K. The DMFT calculations show a genuine Mott insulator without breaking the time-reversal symmetry, whereas the DFT solution requires symmetry breaking to open a gap in the primitive unit-cell calculations. Although the copper network in $CuAl_2O_4$ has a bipartite structure, the paramagnetic ground state persists in the DMFT results. The hole weights are equally distributed in the Kramers pair in Eq. (1) for the entire parameter range considered in this DMFT study. Even if we apply a small staggered magnetic field to stabilize an antiferromagnetic order, the magnetic moment quickly disappears as soon as the staggered field is turned off. The suppression of magnetic order may arise from frustration effects, stemming from larger second-neighbor hopping amplitudes than nearest-neighbor ones [40] (see Supplemental Material [36]). The origin and nature of the nonmagnetic Mott phase of $CuAl_2O_4$ are beyond the scope of the present work. Given the possibility of being extended to the $J_{\rm eff} = 1/2$ spin-glass or -liquid phase, however, the lack of long-range magnetic order is of great interest, requiring further study.

Remarks. A sizable amount of the site disorder between Cu and Al has been recently reported in powder samples of $CuAl_2O_4$ [27]. To check the robustness of the $J_{\rm eff} = 1/2$ picture under disorder, we performed the DFT calculation containing 50% site disorder (see Supplemental Material [36]). Even under the maximal disorder, the single hole at the tetrahedral Cu site preserves the $j_{\rm eff} = 1/2$ character. As shown in Fig. 5S of the Supplemental Material [36], two separated bands appear above the Fermi level, which correspond to the unoccupied Cu *d* orbitals from each tetrahedral and octahedral site. The lower band is perfectly projected onto the $j_{\rm eff} = 1/2$ state in the tetrahedral site, whereas the higher one comes

from the e_g state in the octahedral site. It indicates that the localized unoccupied states in each tetrahedral and octahedral site behave almost independently, indeed manifesting the $J_{\rm eff}$-ness of the tetrahedral Cu^{2+} even with the significant amount of disorder. To understand the spin-glass behavior shown in the powder sample, magnetic interactions under the mixture of tetrahedral site $J_{\rm eff} = 1/2$ and octahedral site e_g states should be studied.

Conclusion. We have shown the theoretical evidence that $CuAl_2O_4$ spinel is a strongly correlated $J_{\rm eff} = 1/2$ Mott insulator. The first-principles total-energy calculations reproduce the previous x-ray data reporting the cubic structure of $CuAl_2O_4$. And its band structure clearly shows that the unoccupied band is well characterized by the $j_{\rm eff} = 1/2$ state. The DMFT calculations uncover the excitation spectra of a strongly correlated $J_{\rm eff} = 1/2$ Mott phase in $CuAl_2O_4$, realizing a $J_{\rm eff} = 1/2$ state in the *LS*-coupling limit.

Acknowledgments. This work was supported by the Institute for Basic Science (IBS) in Korea [Grants No. IBS-R009-D1 (C.H.K., S.B.), No. IBS-R024-D1 (A.G.), No. IBS-R009-G1 (H.C., J.G.P.)] and the Basic Science Research Program of the National Research Foundation (NRF) of Korea under Grants No. 2016R1D1A1B03933255, No. 2017M3D1A1040828, and No. 2019R1A2C1010498 (H.J.). The work of G.V.V. and S.V.S. was supported by the Russian Science Foundation (Grant No. 17-12-01207), while D.I.Kh. thanks the Deutsche Forschungsgemeinschaft (Grant No. SFB 1238) and German Excellence Initiative.

[1] M. Imada, A. Fujimori, and Y. Tokura, Rev. Mod. Phys. **70**, 1039 (1998).
[2] K. I. Kugel and D. I. Khomski, Sov. Phys. Usp. **25**, 231 (1982).
[3] D. I. Khomskii, *Transition Metal Compounds* (Cambridge University Press, Cambridge, 2014).
[4] B. J. Kim, H. Jin, S. J. Moon, J.-Y. Kim, B.-G. Park, C. S. Leem, J. Yu, T. W. Noh, C. Kim, S.-J. Oh, J.-H. Park, V. Durairaj, G. Cao, and E. Rotenberg, Phys. Rev. Lett. **101**, 076402 (2008).
[5] B. J. Kim, H. Ohsumi, T. Komesu, S. Sakai, T. Morita, H. Takagi, and T. Arima, Science **323**, 1329 (2009).
[6] K. W. Plumb, J. P. Clancy, L. J. Sandilands, V. V. Shankar, Y. F. Hu, K. S. Burch, H.-Y. Kee, and Y.-J. Kim, Phys. Rev. B **90**, 041112(R) (2014).
[7] H.-S. Kim, J. Im, M. J. Han, and H. Jin, Nat. Commun. **5**, 3988 (2014).
[8] G. Jackeli and G. Khaliullin, Phys. Rev. Lett. **102**, 017205 (2009).
[9] F. Wang and T. Senthil, Phys. Rev. Lett. **106**, 136402 (2011).
[10] Y. K. Kim, O. Krupin, J. D. Denlinger, A. Bostwick, E. Rotenberg, Q. Zhao, J. F. Mitchell, J. W. Allen, and B. J. Kim, Science **345**, 187 (2014).
[11] A. Shitade, H. Katsura, J. Kuneš, X.-L. Qi, S.-C. Zhang, and N. Nagaosa, Phys. Rev. Lett. **102**, 256403 (2009).
[12] C. H. Kim, H. S. Kim, H. Jeong, H. Jin, and J. Yu, Phys. Rev. Lett. **108**, 106401 (2012).
[13] J. Chaloupka, G. Jackeli, and G. Khaliullin, Phys. Rev. Lett. **105**, 027204 (2010).
[14] K. Kitagawa, T. Takayama, Y. Matsumoto, A. Kato, R. Takano, Y. Kishimoto, S. Bette, R. Dinnebier, G. Jackeli, and H. Takagi, Nature (London) **554**, 341 (2018).
[15] S. M. Winter, A. A. Tsirlin, M. Daghofer, J. van den Brink, Y. Singh, P. Gegenwart, and R. Valentí, J. Phys.: Condens. Matter **29**, 493002 (2017).
[16] X. Wan, A. M. Turner, A. Vishwanath, and S. Y. Savrasov, Phys. Rev. B **83**, 205101 (2011).
[17] A. Go, W. Witczak-Krempa, G. S. Jeon, K. Park, and Y. B. Kim, Phys. Rev. Lett. **109**, 066401 (2012).
[18] J. G. Rau, E. K.-H. Lee, and H.-Y. Kee, Annu. Rev. Condens. Matter Phys. **7**, 195 (2016).
[19] W. Witczak-Krempa, Y. B. Kim, and L. Balents, Annu. Rev. Condens. Matter Phys. **5**, 57 (2013).
[20] C. Martins, M. Aichhorn, and S. Biermann, J. Phys.: Condens. Matter **29**, 263001 (2016).
[21] H. Liu and G. Khaliullin, Phys. Rev. B **97**, 014407 (2018).
[22] R. Sano, Y. Kato, and Y. Motome, Phys. Rev. B **97**, 014408 (2018).
[23] A. Abragam and B. Bleaney, *Electron Paramagnetic Resonance of Transition Ions* (Clarendon Press, Oxford, 1970).
[24] J. P. Perdew, A. Ruzsinszky, G. I. Csonka, O. A. Vydrov, G. E. Scuseria, L. A. Constantin, X. Zhou, and K. Burke, Phys. Rev. Lett. **100**, 136406 (2008).
[25] http://elk.sourceforge.net
[26] S. L. Dudarev, G. A. Botton, S. Y. Savrasov, C. J. Humphreys, and A. P. Sutton, Phys. Rev. B **57**, 1505 (1998).
[27] R. Nirmala, K.-H. Jang, H. Sim, H. Cho, J. Lee, N.-G. Yang, S. Lee, R. M. Ibberson, K. Kakurai, M. Matsuda, S.-W. Cheong, and J.-G. Park, J. Phys.: Condens. Matter **29**, 13LT01 (2017).
[28] G.-Q. Liu, V. N. Antonov, O. Jepsen, and O. K. Andersen, Phys. Rev. Lett. **101**, 026408 (2008).
[29] D. Pesin and L. Balents, Nat. Phys. **6**, 376 (2010).
[30] M. Cococcioni and S. de Gironcoli, Phys. Rev. B **71**, 035105 (2005).
[31] N. Marzari and D. Vanderbilt, Phys. Rev. B **56**, 12847 (1997).
[32] I. V. Solovyev, P. H. Dederichs, and V. I. Anisimov, Phys. Rev. B **50**, 16861 (1994).
[33] H. Park, A. J. Millis, and C. A. Marianetti, Phys. Rev. Lett. **109**, 156402 (2012).
[34] K. Haule, T. Birol, and G. Kotliar, Phys. Rev. B **90**, 075136 (2014).
[35] M. Caffarel and W. Krauth, Phys. Rev. Lett. **72**, 1545 (1994).
[36] See Supplemental Material at http://link.aps.org/supplemental/10.1103/PhysRevB.100.161104 for calculational details.
[37] R. Arita, J. Kuneš, A. V. Kozhevnikov, A. G. Eguiluz, and M. Imada, Phys. Rev. Lett. **108**, 086403 (2012).
[38] H. Zhang, K. Haule, and D. Vanderbilt, Phys. Rev. Lett. **111**, 246402 (2013).
[39] E. M. Pärschke, K. Wohlfeld, K. Foyevtsova, and J. van den Brink, Nat. Commun. **8**, 686 (2017).
[40] D. Bergman, J. Alicea, E. Gull, S. Trebst, and L. Balents, Nat. Phys. **3**, 487 (2007).